Electronic Supplementary Information

Realizing 6.7 wt% reversible storage of hydrogen at ambient temperature with non-confined ultrafine magnesium hydride

Xin Zhang,[a] Yongfeng Liu,*[a] Zhuanghe Ren,[a] Xuelian Zhang,[a] Jianjiang Hu,[b] Zhenguo Huang,[c] Yunhao Lu,[d] Mingxia Gao[a] and Hongge Pan[a]

[a]State Key Laboratory of Silicon Materials and School of Materials Science and Engineering, Zhejiang University, Hangzhou 310027, China.
*E-mail: mselyf@zju.edu.cn*

[b]School of Chemistry and Chemical Engineering, Yantai University, Yantai 264005, China.

[c]School of Civil & Environmental Engineering, University of Technology Sydney, 81 Broadway, Ultimo, NSW, 2007, Australia.

[d]Zhejiang Province Key Laboratory of Quantum Technology and Device, Department of Physics, Zhejiang University, Hangzhou 310027, China
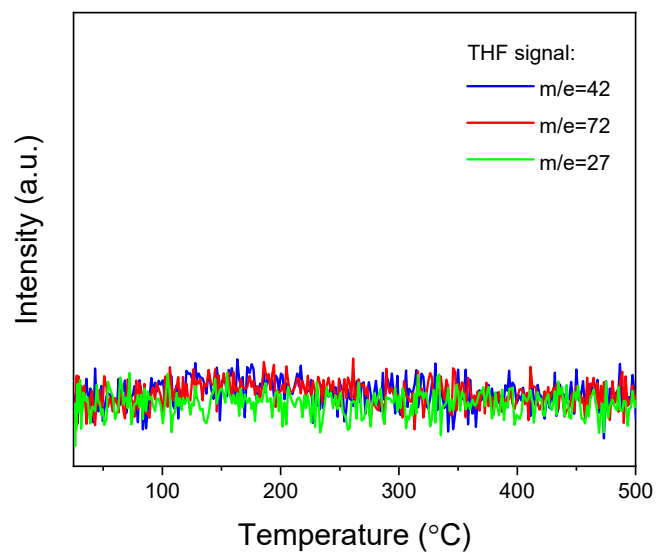
Fig. S1. MS signals of THF in the gaseous products of prepared ultrafine MgH$_2$ nanoparticles with temperatures.
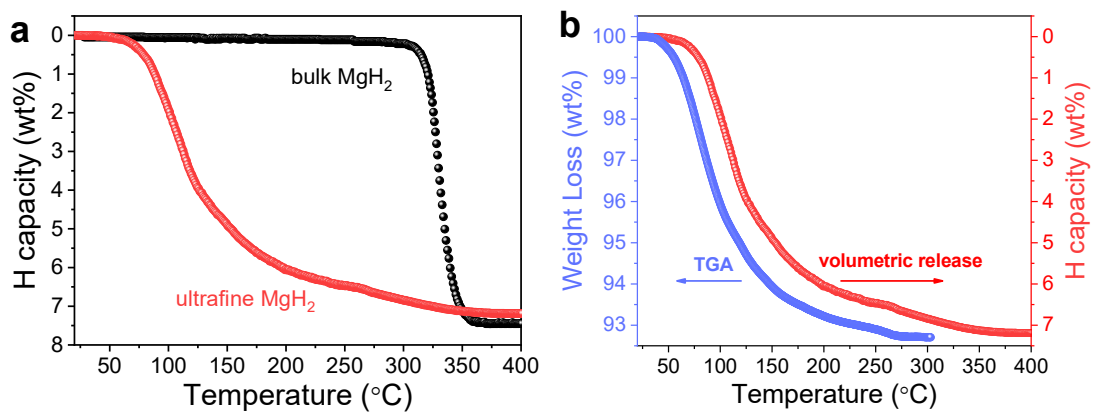
Fig. S2. Volumetric hydrogen release from bulk MgH$_2$ and ultrafine MgH$_2$ (a) and dehydrogenation determined by volumetric release and TGA measurement, respectively (b).
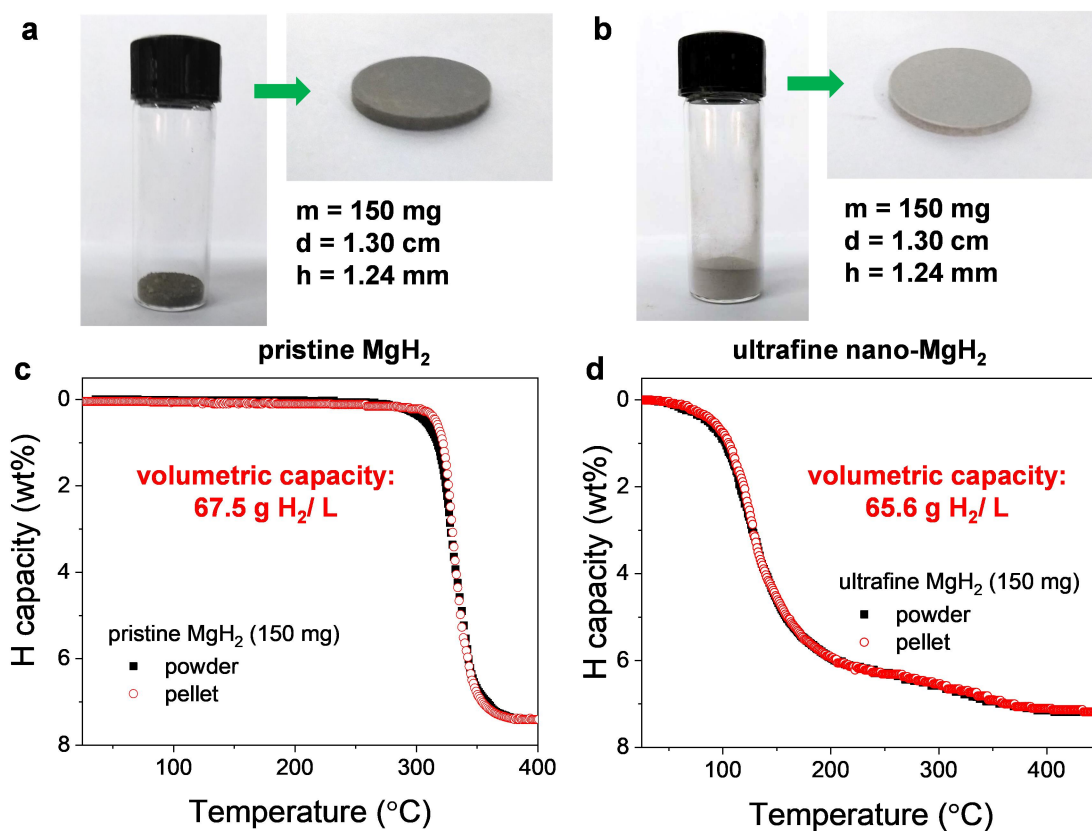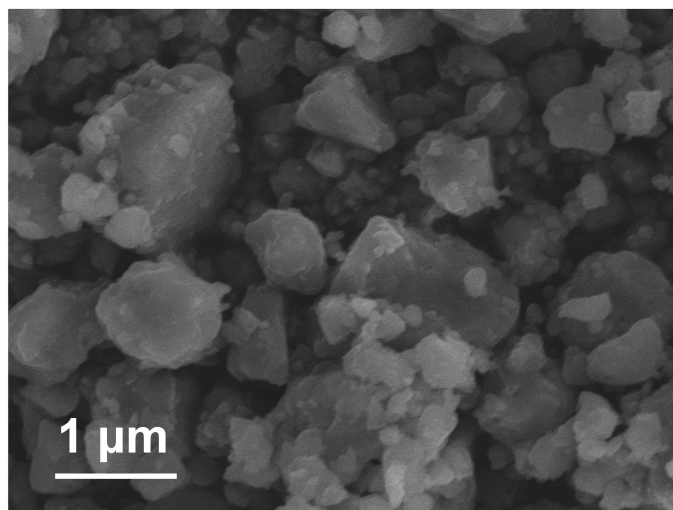
Fig. S3. Digital images (a, b) and volumetric hydrogen release curves (c, d) of pristine (a, c) and ultrafine (b, d) MgH₂ samples in both powder and pellet forms.
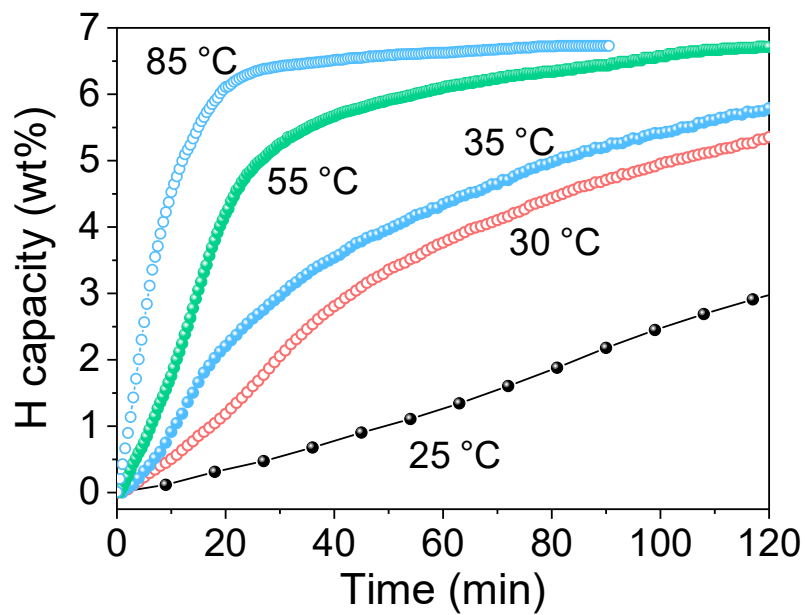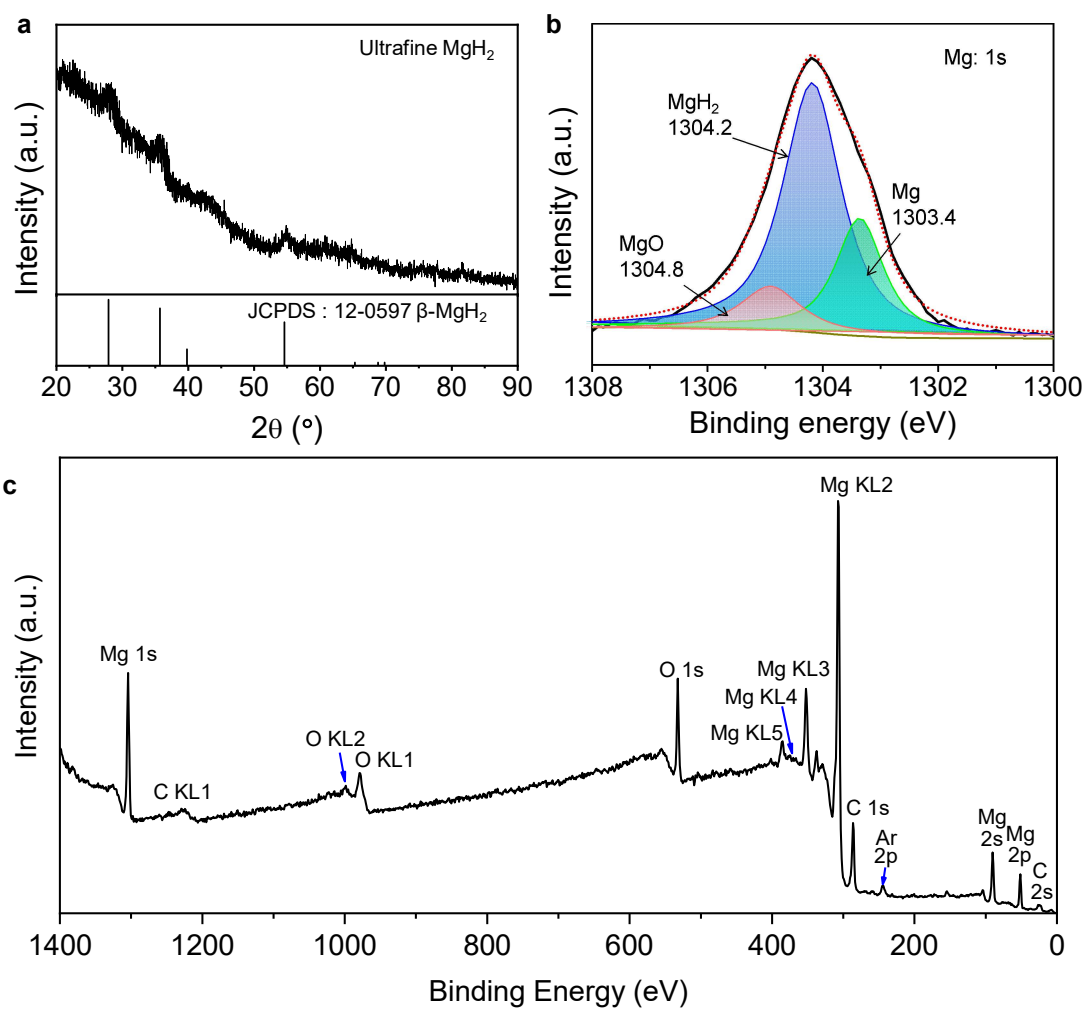
Fig. S4. Isothermal hydrogenation curves of dehydrogenated non-confined ultrafine MgH$_2$ at 25-85 °C under 30 bar H$_2$.
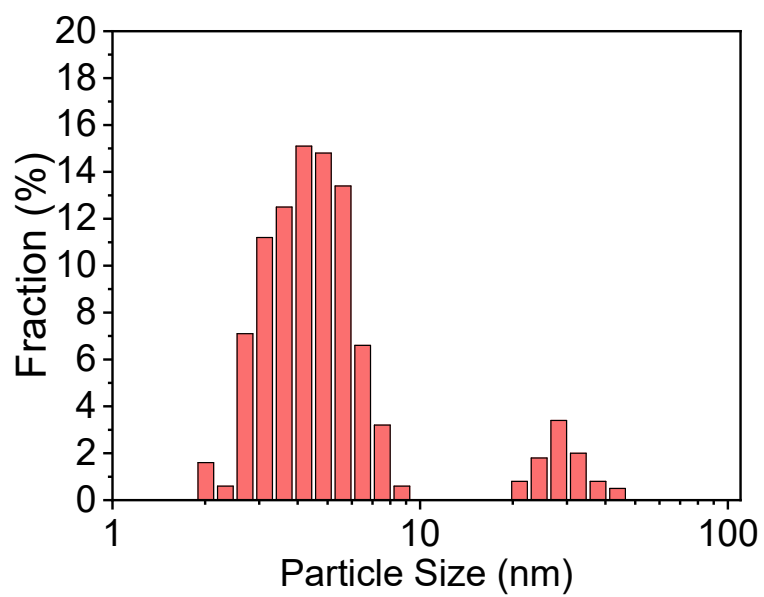
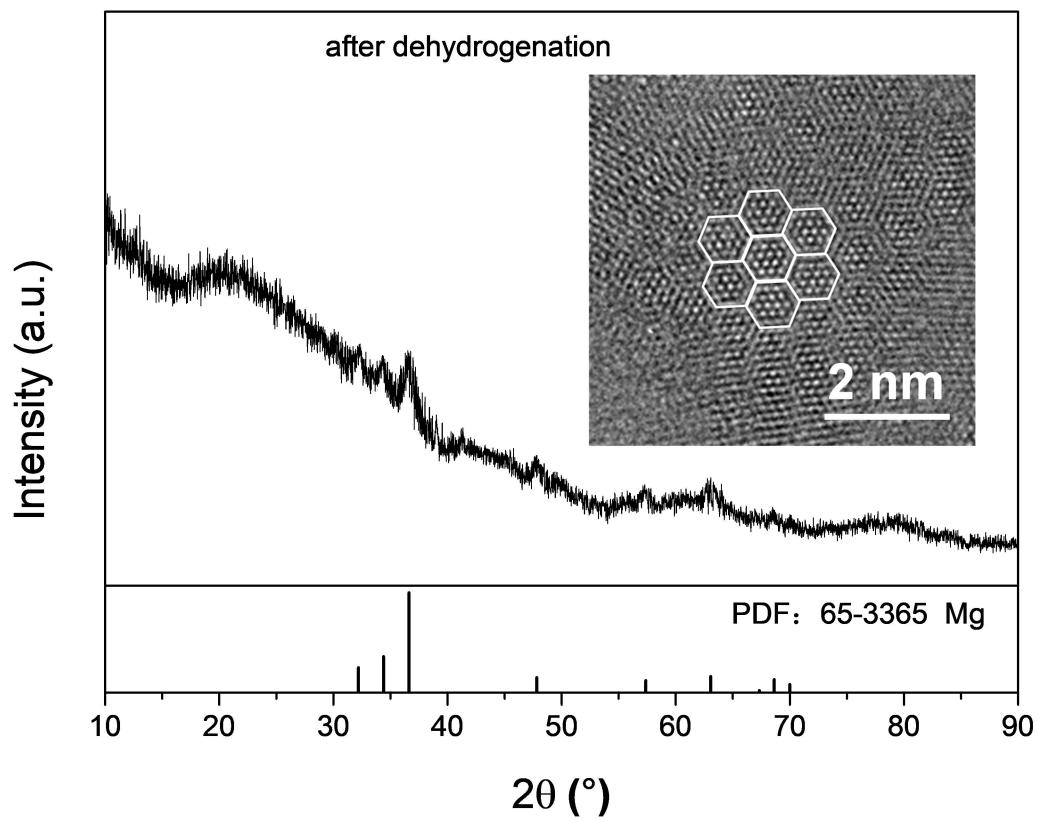**Fig. S5.** Particle size distribution ultrafine MgH_2 prepared after 2 h of sonication treatment.

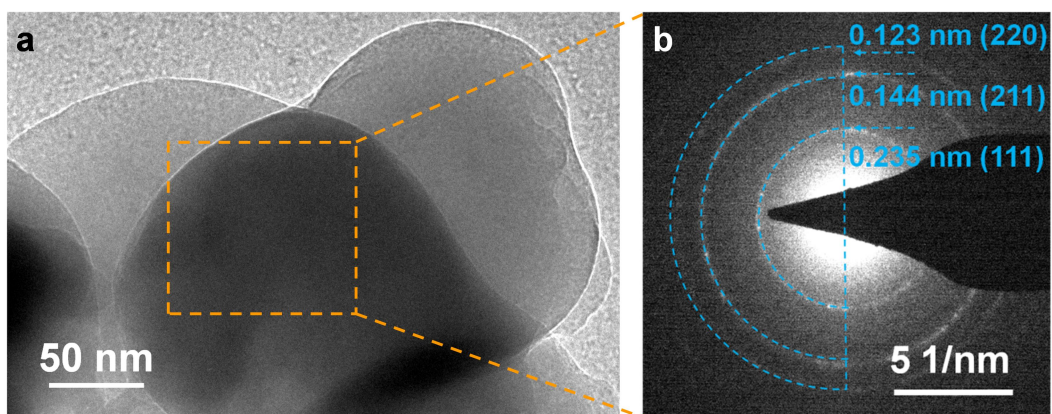**Fig. S6**. SEM image of bulk MgH$_2$ after 24 h of ball milling.

Fig. S7. XRD pattern of non-confined ultrafine MgH$_2$ (a), the corresponding high-resolution XPS spectrum of Mg 1s (b) and XPS survey spectrum collected at 15 °C (c).
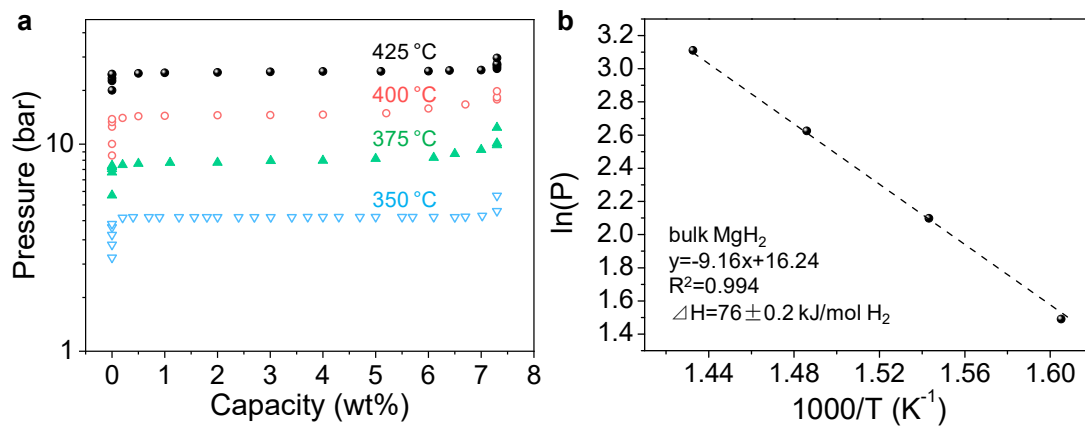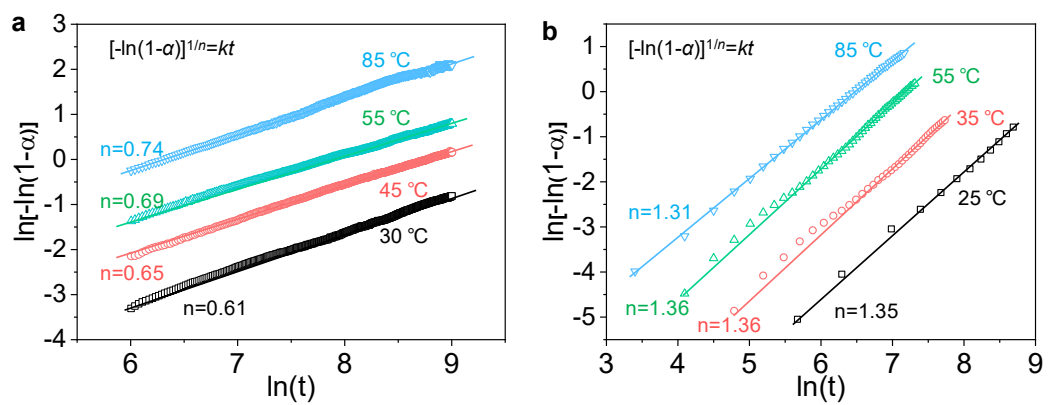
Fig. S8. XRD pattern and HRTEM image (insert) of ultrafine MgH_2 after dehydrogenation.

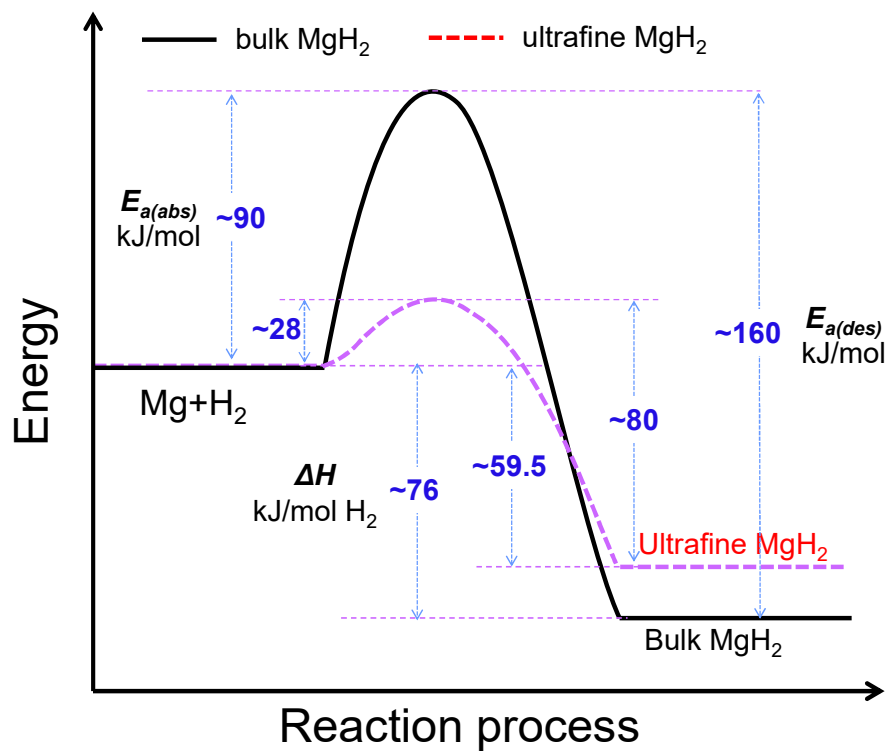**Fig. S9.** TEM images (a) and SAED pattern (b) of LiH without sonication.

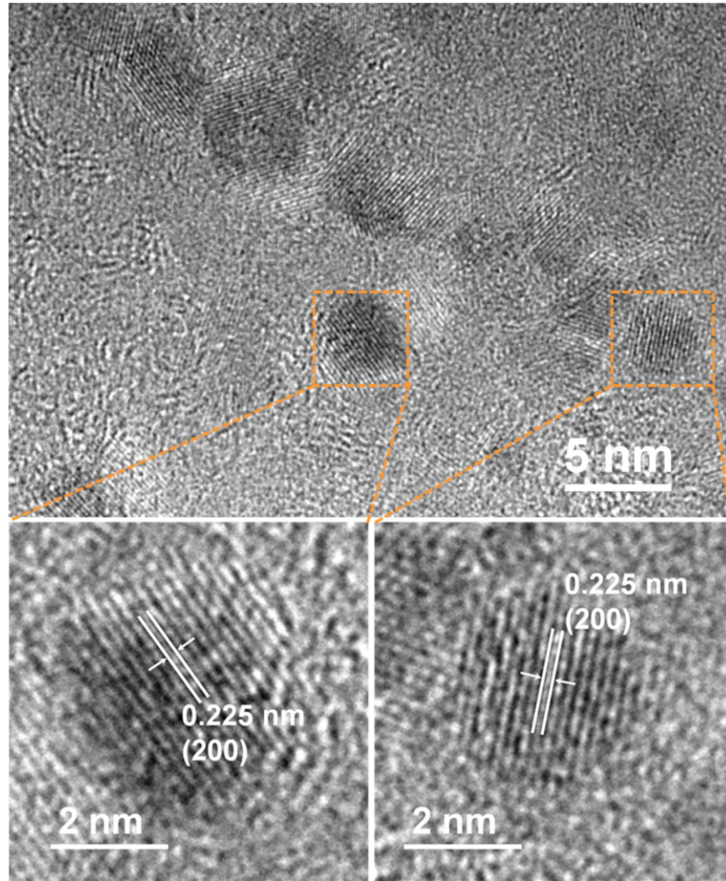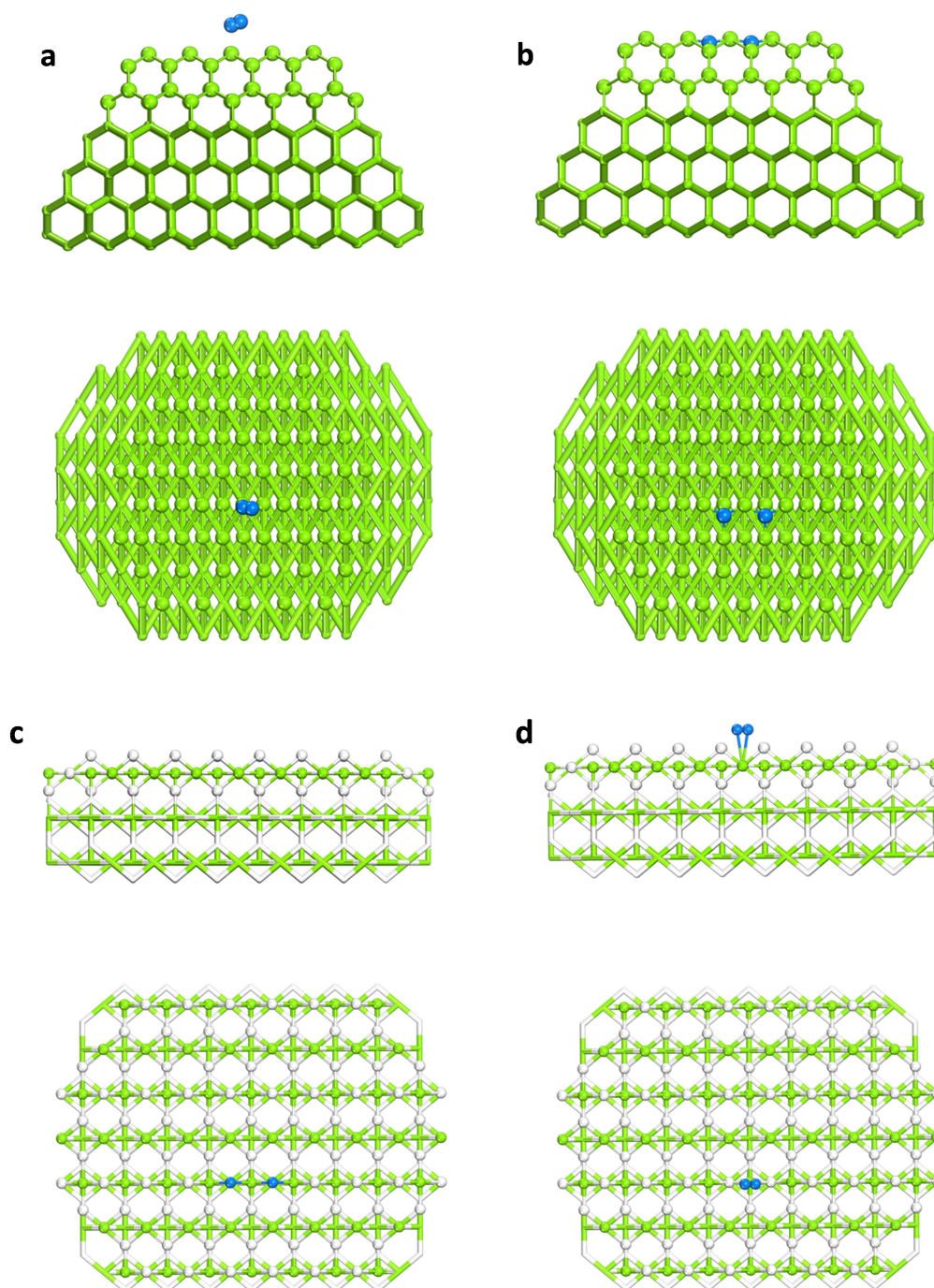**Fig. S10.** PCI measurements (a) and van't Hoff plots (b) for bulk MgH$_2$ at 325-425 °C.

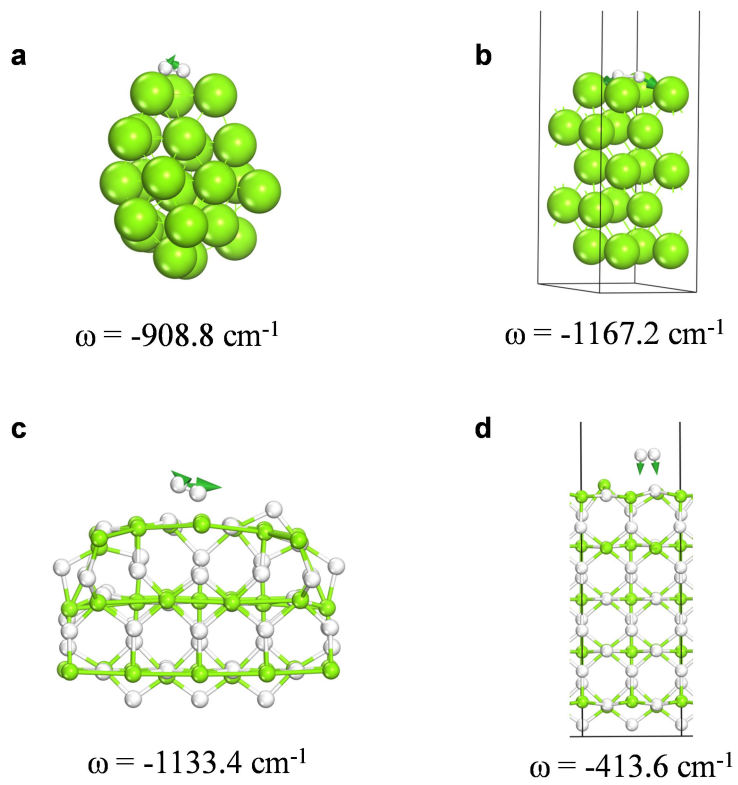**Fig. S11**. JMA plots of non-confined ultrafine MgH_2 for dehydrogenation (a) and hydrogenation (b).

Fig. S12. Comparison of the energy barriers for the hydrogen absorption and desorption of bulk MgH$_2$ and non-confined ultrafine MgH$_2$.

Fig. S13. HRTEM images of non-confined ultrafine MgH$_2$ after 50 cycles.

Fig. S14. DFT calculations of 3 nm clusters. Side and top view before H_2 dissociation (a) and H atoms incorporated into Mg cluster after dissociation (b). The reaction energy of H_2 absorption over 3 nm Mg cluster was calculated to be -0.43 eV. Side and top view before H desorption (c) and for H_2 released (d). The reaction energy of H_2 desorption from 3 nm MgH_2 cluster was calculated to be 0.89 eV. Mg and H are shown as green and blue spheres.

a

$\omega = -908.8 \text{ cm}^{-1}$

b

$\omega = -1167.2 \text{ cm}^{-1}$

c

$\omega = -1133.4 \text{ cm}^{-1}$

d

$\omega = -413.6 \text{ cm}^{-1}$

Fig. S15. Calculated frequency eigenvalue for the transition states of hydrogen absorption by Mg cluster (a) and slab (b), and hydrogen desorption from MgH_2 cluster (c) and slab (d).

Table S1. Dehydrogenation equilibrium pressures of bulk MgH_2 and non-confined ultrafine MgH_2 at various temperatures

Temperature (°C)	Equilibrium pressure (bar)	
	ultrafine MgH_2 (measured)	bulk MgH_2 (calculated)[a]
80	3.8×10^{-3}	7.5×10^{-5}
100	0.0108	3×10^{-4}
120	0.0304	1.05×10^{-3}
160	0.151	7.37×10^{-3}
215	1.014	0.095
220	1.210	0.096

[a]Calculations were carried out according to the van't Hoff equation shown in Fig. S10 b.